# Laser generation of hypersound by a terahertz photo-Dember electric field in a piezoelectric GaAs semiconductor

Gwenaelle Vaudel,[1] Thomas Pezeril,[1,*] Alexei Lomonosov,[1,†] Marius Lejman,[1] Pascal Ruello,[1] and Vitalyi Gusev[1,2,‡]

[1]*Institut Molécules et Matériaux du Mans, UMR CNRS 6283, Université du Maine, 72085 Le Mans, France*

[2]*Laboratoire d'Acoustique de l'Université du Maine, UMR CNRS 6613, Université du Maine, 72085 Le Mans, France*

(Received 23 December 2013; revised manuscript received 20 June 2014; published 9 July 2014)

We experimentally demonstrate the optical generation of hypersound in a piezoelectric GaAs semiconductor through laser excitation of the THz photo-Dember electric field. Such an ultrashort transient Dember electric field is linked to the spatial separation of photoexcited electrons and holes right after above-band-gap femtosecond laser excitation. Through time-domain coherent Brillouin scattering we demonstrate that photoinduced piezoelectric generation of hypersound can dominate even in the absence of preexisting built-in fields and we observe, with increasing laser fluence, a nonlinear optoacoustic excitation process. These results reveal the onset of the THz photo-Dember electric field and highlight the transition from non-ambipolar flow to ambipolar diffusion of the photoexcited electron-hole plasma.

DOI: 10.1103/PhysRevB.90.014302 PACS number(s): 78.20.H−, 72.50.+b, 78.20.N−, 78.47.−p

Investigation of the physical mechanisms behind ultrafast optical generation of acoustic phonons is an important subfield in solid state physics [1–6]. In particular, picosecond laser ultrasonics [2], a technique where femtosecond laser pulses are applied for both optical generation and detection of acoustic phonons in the GHz-THz frequency range [2–6], provides a wealth of information on the ultrafast physical processes following femtosecond laser-matter interaction. Optical generation of hypersound from the inverse piezoelectric effect following the laser screening of built-in electric fields has been demonstrated in the past [3,4], and more recently in multiple and single semiconductor quantum wells [7–13], at surfaces and interfaces (p-n junctions) [14–20], in multiple quantum well p-i-n diodes under application of an external bias [21,22], and in ferroelectrics [23,24]. These experiments provided crucial information on the onset of ultrafast screening dynamics of preexisting stationary electric fields by photogenerated charge carriers in piezoelectric materials. Nonlinear ultrafast optical generation of acoustic phonons at increasing pump laser fluence has been observed and attributed to the saturation of the inverse piezoelectric effect at full screening of the built-in field [8,11–13,15,17–20,23]. All these observations related to optoacoustic excitation in piezoelectric materials were limited to the experimental situations of preexisting built-in field [6–24]. Here we report the observation of nonlinear optoacoustic conversion in nondoped piezoelectric GaAs wafers with negligible built-in fields. In this specific situation, we demonstrate that the nonlinear optoacoustic conversion is caused by the saturation of the photo-Dember THz electric field [25,26] created by the ultrafast separation of photoexcited charges of different diffusivities. Our findings demonstrate the competition of the inverse piezoelectric effect (PE) (related to the photo-Dember THz field) with the electron-hole-phonon deformation potential (DP) optoacoustic mechanism, and reveal the ultrafast spatiotemporal dynamics of the photoexcited charges at the Maxwell relaxation time scale and at the Debye screening length scale [27].

For the pump-probe femtosecond experiment, a Ti-sapphire oscillator running at a repetition rate of 80 MHz was used to generate laser pulses with central wavelength of 800 nm and 150 fs duration. The laser output was split into separate pump and probe beams. The pump beam was frequency-doubled by a second harmonic generation BBO crystal in order to obtain a pump wavelength of 400 nm. The experiments were performed on the opposite faces A (111) and B ($\bar{1}\bar{1}\bar{1}$) of a nondoped GaAs wafer. Given the residual n-type doping of nondoped GaAs about $10^8$ cm$^{-3}$, the corresponding built-in field is $10^5$ times lower than in the experiments cited above and therefore can be neglected [28]. At 400 nm pump light, the GaAs optical penetration depth is $1/\alpha = 14$ nm while at 800 nm probe light it is over 1 $\mu$m. Both pump and probe beams were focused at normal incidence on the sample surface. A spinning wedge mirror device was used in order to continuously move the pump-probe spots on the sample surface during acquisition; see Fig. 1. The ring trajectory of the moving spots is about 100 $\mu$m in diameter and the spinning frequency is in the range of 50 Hz. In fact by lowering the laser repetition rate, our simple spinning wedge mirror device could be used to perform single-shot types of experiments at high speed [29]. Currently, this technique avoids unwanted sample damage and remarkably extends the sample lifetime.

Absorption of the femtosecond laser pump causes sudden lattice expansion [in the case of DP for both faces or PE on face B ($\bar{1}\bar{1}\bar{1}$)] or contraction [in the case of PE on face A (111)], which launches an ultrashort longitudinal acoustic pulse in the GaAs substrate. The probe light which enters the relatively semitransparent GaAs substrate is partially scattered by the propagating longitudinal acoustic pulse. The coherently scattered field, whose optical phase varied depending on the acoustic wave position, superposed with the probe field reflected at the free surface, results in signal intensity that shows time-dependent Brillouin oscillations; see Fig. 2. Consequently, the oscillatory component of the measured transient reflectivity signals can be described by

$$\Delta R(t) = C\cos(\omega t - \phi), \tag{1}$$

*thomas.pezeril@univ-lemans.fr

†Current address: General Physics Institute, Russian Academy of Sciences, Moscow, Russia.

‡vitali.goussev@univ-lemans.fr

 

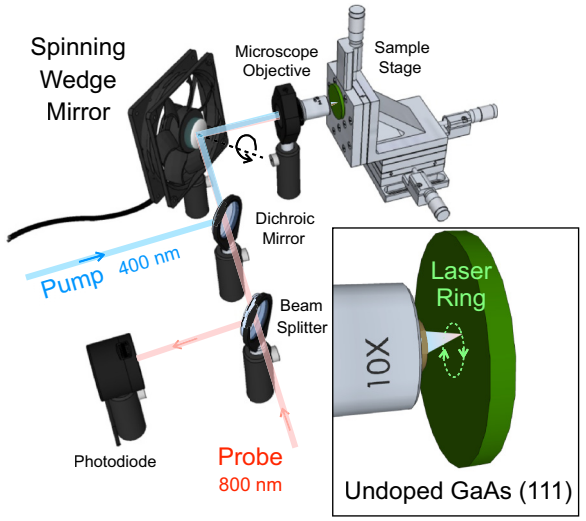


FIG. 1. (Color online) Sketch of the femtosecond pump-probe experimental setup. Both 400 nm pump and 800 nm probe beams are focused at normal incidence on the GaAs (111) sample surface. The continuously spinning wedge mirror right in front of the microscope objective is used to cycle at high speed the pump-probe acquisition along the sample surface; see inset. At the focus of the 10× microscope objective, the pump-probe spot positions follow a ring trajectory. This operation allows the measurement to be continuously sampled over different pump-probe positions on the sample surface and prevents the sample from laser damage or curing.

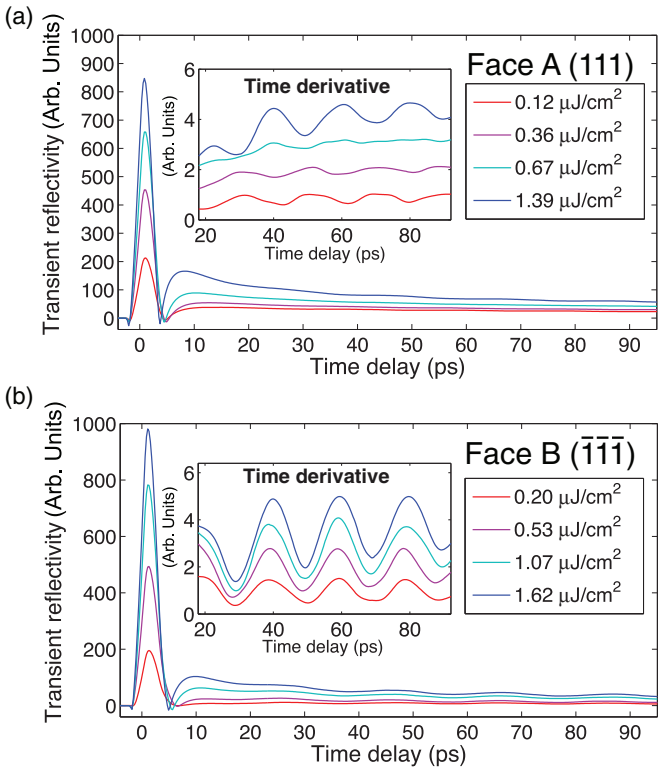


FIG. 2. (Color online) Transient reflectivity signals obtained for both faces (a) A (111) and (b) B ($\bar{1}\bar{1}\bar{1}$) of nondoped GaAs for different pump fluences on a picosecond time scale. The insets in (a) and (b) display the time derivative of the transient reflectivity signals and highlight the Brillouin oscillations. The vertical unit of both figures is identical, meaning that both signal amplitudes (a) and (b) can be compared. In both cases, while the "electronic peak" at 0 ps time delay linearly increases with increasing laser pump fluence, the Brillouin oscillations in the insets behave differently; in particular a discrepancy between A and B can be clearly noticed for the Brillouin amplitude and phase changes at increasing laser pump fluence.

where $\omega = 2\pi\nu$ is the Brillouin angular frequency, and $C$ and $\phi$ are the amplitude and the phase of the Brillouin oscillations. The transient reflectivity results shown in Fig. 2 clearly indicate that the Brillouin oscillations behave differently at the opposite faces A (111) and B ($\bar{1}\bar{1}\bar{1}$) of the GaAs sample and depend on the laser pump fluence. It is not only the Brillouin amplitude but also the Brillouin phase which clearly appears to be dependent on the laser pump fluence in the case of A (111); see the time derivative in Fig. 2(a).

A full set of transient reflectivity data covering a broad fluence range from 0.015 $\mu$J/cm$^2$ to 1.4 $\mu$J/cm$^2$ has been acquired. After time derivation and FFT analysis of the 49 GHz Brillouin frequency, as in [30], both amplitudes and phases have been extracted at all measured fluences; see Figs. 3(a) and 3(b). By definition, the laser pump fluence is taken as the laser pump pulse energy divided by $\pi d^2/4$ where $d = 20$ $\mu$m is the diameter at the $1/e^2$ intensity level at the pump spot focus. In the case of built-in fields in the range of 10–100 kV/cm, the typical laser fluence range is between $F_L \approx$ 5–10 $\mu$J/cm$^2$, which is significantly higher than in the present case dealing with THz Dember fields. As a matter of fact, since the piezoelectric moduli are of opposite sign between A and B (see Appendix A), while the deformation potential constants remain unchanged, the spectacular nonmonotonic behavior of the Brillouin oscillations on face A, in particular the singularity at 0.6 $\mu$J/cm$^2$ in Fig. 3(a) where the Brillouin oscillations vanish, evidences the competition between PE and DP mechanisms for hypersound generation. In addition, the nearly antiphase oscillations on faces A compared to B, at low pump fluences, indicate the dominance of the inverse PE and the nearly in-phase oscillations on both faces at high fluences indicate the dominance of the DP over the PE mechanism; see Figs. 3(a) and 3(b).

By assuming that the only difference between faces A and B is the sign change of the piezoelectric modulus, each separate DP or PE contribution can be extracted from the experimental data based on the following equation:

$$\begin{aligned}\Delta R^{A,B} &= C^{A,B}\cos(\omega t - \phi^{A,B}) \\ &= C_{\mathrm{DP}}\cos(\omega t - \phi_{\mathrm{DP}}) + C_{\mathrm{PE}}\cos\left(\omega t - \phi_{\mathrm{PE}}^{A,B}\right), \quad (2)\end{aligned}$$

where A and B indicate the face and DP, PE the excitation mechanism. In Eqs. (2), it is implicitly assumed that DP constants are identical for both faces (which implies that $\phi_{\mathrm{DP}}^{A} = \phi_{\mathrm{DP}}^{B} = \phi_{\mathrm{DP}}$ and $C_{\mathrm{DP}}^{A} = C_{\mathrm{DP}}^{B} = C_{\mathrm{DP}}$), and that the piezoelectric modulus changes sign depending on face A or B (which implies that $\phi_{\mathrm{PE}}^{A} = \phi_{\mathrm{PE}}^{B} \pm \pi$ with $C_{\mathrm{PE}}^{A} = C_{\mathrm{PE}}^{B} = C_{\mathrm{PE}}$). This model does not account for additional differences between faces A and B caused by different terminations and reactivities [28]. A fitting procedure has been applied to the experimental data presented in Figs. 3(a) and 3(b), which leads to smoothed experimental functions and $\phi^{A,B}$ that have been substituted into Eqs. (2) in order to calculate $C_{\mathrm{DP}}$ and $C_{\mathrm{PE}}$.

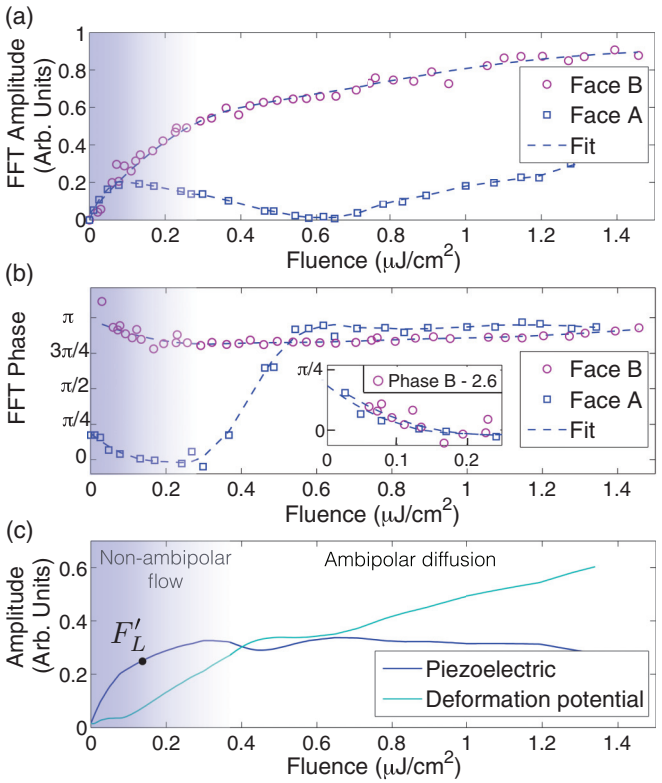


FIG. 3. (Color online) FFT amplitude (a) and phase (b) of the Brillouin oscillations versus the pump fluence for each side A and B of the sample. The inset in (b) highlights the superposition of phase A and phase B, shifted by 2.6 radians. A routine fitting procedure applied to experimental data (a) and (b) was used to extract from Eqs. (2) the amplitude of the PE and DP mechanisms versus the pump fluence (c). Two optoacoustic regimes, linked to non-ambipolar flow at low fluences and ambipolar diffusion at high fluences of the photoexcited charges, are evidenced. $F_L'$ is the estimated fluence threshold of the intermediate regime.

In Fig. 3(c) we present the outcome of this calculation which reveals the separation of the DP and PE amplitudes, $C_{\rm DP}$ and $C_{\rm PE}$, versus the pump laser fluence. An interesting observation in Fig. 3(c) is that the amplitude of hypersound generated by PE saturates at a given fluence, indicating that the photo-Dember field reaches a maximum value and saturates as well, while the DP mechanism always grows with increasing laser fluence. In the following we will discuss the theoretical interpretation of these experimental results in the limiting cases of low fluences (in the range of 0–0.1 $\mu$J/cm$^2$) and high fluences (in the range of 0.6–1.4 $\mu$J/cm$^2$) which can be solved analytically.

At low fluences, due to the localized absorption of laser light and to the high mobility of electrons compared to holes in GaAs [28] (see Appendix B), the regime of non-ambipolar flow of the photoexcited charge carriers is expected; see Fig. 4(a). This regime can be modeled as [31]

$$n_h(z,t)=N_L\delta(z)H(t),\quad n_e(z,t)=\frac{N_L/l_{\rm Debye}}{(1+z/l_{\rm Debye})^2}H(t),$$

$$E_{\rm Dember}(z,t)=E_{h0}\frac{1}{1+z/l_{\rm Debye}}H(t) \qquad (3)$$

$$\text{with}\quad E_{h0}=\frac{|q|N_L}{\epsilon_0\epsilon_r},$$

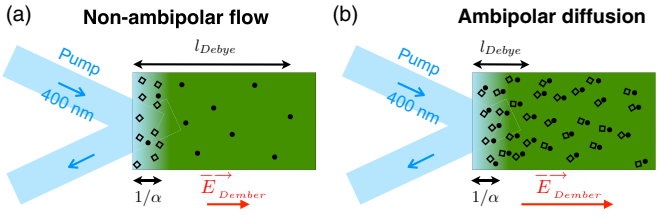


FIG. 4. (Color online) (a) At low fluence, the non-ambipolar flow of photoexcited charges is characterized by the holes' immobility and supersonic electronic flow far away from the photoexcited region (in blue). In this case the Debye screening length follows the inequality $l_{\rm Debye} \gg 1/\alpha$. (b) At higher fluence, the ambipolar diffusion characterized by the simultaneous diffusion of quasineutral electron-hole plasma takes place. In this case the Debye screening length is shorter than the characteristic spatial scale of the electron-hole plasma distribution.

where $n_{h,e}$ is the concentration of electrons (e) and holes (h), $H(t)$ denotes the Heaviside step function, $l_{\rm Debye} = 2D_e/\mu_e E_{h0} \propto 1/N_L$ is the Debye screening length [27] ($D_e$ and $\mu_e$ are the diffusivity and mobility of the charge carriers), $N_L$ is the sheet density of electron-hole pairs which scales linearly with the laser fluence $F_L$ ($N_L \propto F_L$), $\delta(z)$ is the delta function in $z$, and $\epsilon_0$ and $\epsilon_r$ are the vacuum permittivity and the relative permittivity. Equations (3) are valid right when the supersonic flow of electrons is balanced by the drift in the opposite direction from the $E_{h0}$ field created by the holes delta-localized at the surface. The stresses $\sigma_{\rm PE} = -p_E\, E_{\rm Dember}$ and $\sigma_{\rm DP} = -d_e n_e - d_h n_h$ calculated from Eqs. (3), where $p_E$ is the piezoelectric modulus and $d_e$ and $d_h$ are the deformation potential coefficients of electrons and holes (see Appendix A), lead to the prediction of the laser-generated strain waves. Our theory predicts generation of bipolar antisymmetric longitudinal acoustic pulses of duration equal to twice the time of sound propagation across the Debye screening length. The evaluation of the acoustic spectrum at the Brillouin angular frequency outcomes $\phi^A_{\rm DP} = \phi^B_{\rm DP} = \phi^B_{\rm PE} = \pi$, $\phi^A_{\rm PE} = 0$, and $C_{\rm PE} \sim 8\, C_{\rm DP}$ is valid up to 0.05 $\mu$J/cm$^2$. These estimates corroborate our experimental observations of $C_A \approx C_B$, $\phi_A \approx 0$, $\phi_B \approx \pi$, see Figs. 3(a) and 3(b), and validate the observation of an efficient increase of PE compared to DP in the fluence range of 0–0.05 $\mu$J/cm$^2$, see Fig. 3(c). To account for the specific time $\tau_{\rm Maxwell}$ of the electron-hole separation during the onset of the Dember electric field, the Heaviside step function $H$ can be changed for $1-\exp(-t/\tau_{\rm Maxwell})$ in Eqs. (3). This time necessary to stop the supersonic flow of electrons induces an additional phase shift $\Delta\phi = \arctan(\omega\tau_{\rm Maxwell})$ of the Brillouin oscillations. Consequently, the experimental observation of a phase shift up to $\Delta\phi \approx \pi/6$, see inset Fig. 3(b) at the lowest fluences below 0.1 $\mu$J/cm$^2$, illustrates the process of Maxwell relaxation of the non-ambipolar flow of electrons and can be used to evaluate $\tau_{\rm Maxwell} \approx 2$ ps.

In the asymptotic case of high laser fluence, where the ambipolar diffusion of the e-h plasma occurs, the analysis of the optoacoustic generation at the Brillouin frequency can be importantly simplified taking into account that the diffusion length $l_D = 2\sqrt{Dt}$, where $D = (\mu_e D_e + \mu_h D_h)/(\mu_e + \mu_h)$ is the ambipolar diffusivity, is ten times the light penetration depth $1/\alpha$ at the time scale of the Brillouin period.

Consequently the plasma concentration $n$ can be estimated assuming delta-localized surface absorption of the laser pump and in depth diffusion of the carriers which leads to the corresponding transient Dember field,

$$\begin{aligned} n(z,t) &\cong (N_L/\sqrt{\pi Dt})\exp[-z^2/(4Dt)]H(t), \\ E_{\text{Dember}}(z,t) &\cong \frac{z}{2Dt}\frac{D_e-D_h}{\mu_e-\mu_h}[H(z)-H(z-l_c)]H(t), \end{aligned} \tag{4}$$

where the critical length $l_c \approx 1.7\,l_D$ (see Appendix B). It can be noted that $E_{\text{Dember}}$ in Eq. (4) no longer depends on the fluence. The factor $H(z)-H(z-l_c)$ expresses the fact that the Dember field is linked to the diffusion of the e-h plasma and vanishes outside the diffusion depth of the carriers; see Fig. 4(b). The laser-generated strain waves can be deduced from the above model for $n(z,t)$ and $E_{\text{Dember}}(z,t)$. Due to the supersonic nature of the ambipolar diffusion, which implies the inequality $\omega_D \equiv v_a^2/D \ll \omega$ [15], the solutions can be simplified to the first-order expansion. Finally, we obtain a reliable theoretical interpretation of the dominance of the DP mechanism over the inverse PE at high fluences. Our theory also explains the observed transition from $\phi_B > \phi_A$ at low fluences to $\phi_B < \phi_A$ at high fluences; see Fig. 3(a). In fact the theoretical predictions for phases are $\phi_{\text{DP}} = 3\pi/4 + \arctan(\omega_D/\omega) \approx 3\pi/4$, $\phi_{\text{PE}}^A = 3\pi/2 + \arctan[\cos(a^2\omega^2/2\omega_D^2)/2] > \phi_{\text{DP}}$, and $\phi_{\text{PE}}^B = \phi_{\text{PE}}^A - \pi < \phi_{\text{DP}}$ (see Appendix B). Since $\phi_{\text{PE}}^B < \phi_{\text{DP}} < \phi_{\text{PE}}^A$, the PE contributions drive the phase of the Brillouin oscillation down on face B and up on face A, inducing experimentally observed $\phi^B < \phi^A$ at high fluences; see Fig. 3(a) in the fluence range 0.6–1.4 $\mu$J/cm$^2$.

In the intermediate regime, at the transition from non-ambipolar flow to ambipolar diffusion, both models can be interpolated. With increasing fluence, the Debye screening length shortens such that the inequality $l_{\text{Debye}} \propto 1/F_L \gg 1/\alpha$ of the non-ambipolar flow is no longer valid. However, from the criterium $l_{\text{Debye}} = 2/\alpha$, we can estimate the threshold sheet density $N_L'$ and corresponding fluence $F_L'$ and $E_{h0}'$ electric field at the intermediate regime from the non-ambipolar flow model. We obtain $F_L' \approx 0.14$ $\mu$J/cm$^2$ and $E_{h0}' = |q|N_L'/\epsilon_0\epsilon_r \simeq 21$ kV/cm. Above $F_L'$ the classical ambipolar diffusion of the electron-hole plasma, characterized by $E_{\text{Dember}}(z,t) \equiv -(D_e-D_h)(\partial n/\partial z)/(\mu_e-\mu_h)n$, is expected to take place [27]. In fact the Dember field of the ambipolar diffusion process is maximum when the plasma concentration is constrained over the optical skin depth area; in this case $n \sim \exp(-\alpha z)$ and $E_{\text{Dember}} = \alpha(D_e-D_h)/(\mu_e-\mu_h) \simeq 18$ kV/cm is practically equal to the $E_{h0}'$ field of the non-ambipolar flow. This indicates that above the critical fluence $F_L'$ the saturation of the photo-Dember field occurs. Our estimate of $F_L' \approx 0.14$ $\mu$J/cm$^2$ is in reasonable agreement with the experimentally observed saturation threshold of 0.2 $\mu$J/cm$^2$ for $C_{\text{PE}}$ in Fig. 3(c), which proves the accuracy of our model and the link between the optoacoustic amplitude $C_{\text{PE}}$ and the onset of the ambipolar diffusion.

Our experimental observations are adequately correlated to the transition from non-ambipolar flow to ambipolar diffusion of photoexcited charges with increasing laser fluence. The developed theoretical models provide correct estimates for the characteristic laser fluence at which we observed peculiar nonlinear behavior of the longitudinal phonon amplitude and phase, very different at opposite faces A or B of the sample. Using time-resolved Brillouin scattering we demonstrate the possibility to extract the Maxwell relaxation time and the Debye screening length of the photoexcited distribution of charges. In this perspective, the application of this technique in piezoelectric-ferroelectric materials could provide access to the dynamics of the laser-induced optoacoustic phenomena at subpicosecond time scales which still remains elusive.

## ACKNOWLEDGMENTS

This work was partially supported by Région des Pays de la Loire and ANR contract GHzOCPETs (6-blanc-0013). We are grateful to Philippe Babilotte and Sergey Avanesyan for assistance in preliminary experiments.

## APPENDIX A: NONDOPED GaAs PARAMETERS

The experiments were performed on the opposite faces A (111) and B ($\bar{1}\bar{1}\bar{1}$) of a nondoped GaAs wafer, with the residual majority carrier (electron) concentration of $n_{e0} = 9.8 \times 10^7 cm^{-3}$ (resistivity $\rho = 1.1 \times 10^9$ $\Omega$m and electron mobility $\mu_e \approx 0.6\,\text{m}^2\,\text{V}^{-1}\,\text{s}^{-1}$). From the typical value of the built-in potential $|q|V_{\text{BI}} \approx 0.8$ eV in n-doped GaAs [32], we can estimate the built-in electric field $|E_{\text{BI}}| \simeq \sqrt{2|q|n_{e0}V_{\text{BI}}/(\epsilon_0\epsilon_r)} \approx 4.4$ V/cm and the sheet concentration of the electrons that could be captured at the surface $N_S \approx \epsilon_0\epsilon_r|E_{\text{BI}}|/|q| = 3.1 \times 10^7$ cm$^{-2}$, which are both extremely low. In these formulas $q$ is the electron charge, $\epsilon_0$ is the dielectric permittivity of vacuum, and $\epsilon_r \approx 13$ is the relative quasistatic dielectric permittivity of GaAs [28,32,33]. The sheet density of the photoexcited carriers can be estimated in our experiments as $N_L = (1-R_b)F_L/(h\nu_b) \approx [F_L/(1\,\mu\text{J cm}^{-2})]10^{12}\,\text{cm}^{-2}$, where $R_b \approx 0.47$ and $h\nu_b \simeq 3.14$ eV are the reflectivity at the air/GaAs interface and the photon energy of the 400 nm laser pump [33]. Thus from the condition $N_L = N_S$ we estimate that the built-in electric field in our nondoped sample can be completely screened at the pump fluence of $F_L \approx 30\,\text{pJ cm}^{-2}$, which is $10^3$ times lower than the minimum fluence in our experiments ($F_L \geqslant 0.015\,\mu\text{J cm}^{-2}$). It can be concluded that the processes of charge separation in the built-in electric field do not contribute to the experimentally observed nonlinear optoacoustic phenomenon.

The [111] direction corresponds to the maximum magnitude of the piezoelectric modulus $p_E = 2p_{14}/\sqrt{3} \approx 0.185$ C/m$^2$. The deformation potentials of electrons and holes are $d_e \approx 7.17$ eV and $d_h \approx 1.16$ eV [28,32,33]. The photoelastic constant is negative ($\partial k'/\partial\eta < 0$) in GaAs with weak residual concentration of electrons in the conduction band at 800 nm probe wavelength. The piezoelectric modulus is negative at face A ($p_E^A < 0$) and positive at face B ($p_E^B > 0$) [28,34].

## APPENDIX B: THEORETICAL ANALYSIS

### 1. Hypersound generation in the process of non-ambipolar flow of photoexcited charge carriers

The system of equations describing drift and diffusion of the photoexcited electrons and holes can be presented in the

form

$$\frac{\partial n_e}{\partial t} - \mu_e \frac{\partial (n_e E)}{\partial z} - D_e \frac{\partial^2 n_e}{\partial z^2} = \alpha N_L \delta(t) \exp(-\alpha z),$$
$$\frac{\partial n_h}{\partial t} + \mu_h \frac{\partial (n_h E)}{\partial z} - D_h \frac{\partial^2 n_h}{\partial z^2} = \alpha N_L \delta(t) \exp(-\alpha z), \quad \text{(B1)}$$
$$\frac{\partial E}{\partial z} = -\frac{|q|}{\epsilon_0 \epsilon_r}(n_e - n_h).$$

Here the femtosecond photo-excitation of the electrons and holes is treated as being delta-localized in time. The third of these equations, the Poisson equation [27,35], describes the creation of the Dember electric field $E(z,t)$ due to the spatial separation of electrons and holes. Note that in this appendix we are using everywhere the notation $E$ instead of $E_{\text{Dember}}$ for compactness of the formulas. Analytical description of the low-fluence regime is possible due to the strong difference between electron and hole mobilities in GaAs ($D_e/D_h \geqslant 15$, $\mu_e > 0.6\,\text{m}^2\,\text{V}^{-1}\,\text{s}^{-1}$, and $\mu_h < 0.04\,\text{m}^2\,\text{V}^{-1}\,\text{s}^{-1}$) [28,32,33]. Assuming that the holes are immobile and localized at the surface, the problem in Eq. (B1) is reduced to the analysis of the electronic flow in the instantaneously induced homogeneous field of the spatially $\delta$-localized holes:

$$\frac{\partial n_e}{\partial t} - \mu_e \frac{\partial (n_e E)}{\partial z} - D_e \frac{\partial^2 n_e}{\partial z^2} = 0, \quad \frac{\partial E}{\partial z} = -\frac{|q|}{\epsilon_0 \epsilon_r} n_e,$$
$$E = E_h + E_e, \quad E_e(t,0) = 0, \quad n_h(t,z) = N_L \delta(z) H(t),$$
$$E_h(t,z) = \frac{|q| N_L}{\epsilon_0 \epsilon_r} H(z) H(t) \equiv E_{h0} H(z) H(t). \quad \text{(B2)}$$

Here $H$ denotes the Heaviside step function. Equations (B2) can be integrated in the stationary limit, i.e., $t \to \infty$, $\partial n_e/\partial t \to 0$,

$$E(z,\infty) = \frac{E_{h0}}{1 + z/l_{\text{Debye}}}, \quad n_e(z,\infty) = \frac{N_L/l_{\text{Debye}}}{[1 + z/l_{\text{Debye}}]^2}. \quad \text{(B3)}$$

Here $l_{\text{Debye}}(N_L) = 2D_e/(\mu_e E_{h0})$ denotes the fluence-dependent Debye screening length [27,35] defined for the fluence-dependent characteristic stationary concentration of the electrons, which in accordance with Eq. (B3) is $n_e(\infty) = N_L/l_{\text{Debye}}(N_L) \propto N_L^2$. The solutions (B3) describe the distributions of the electric field and the concentration of the photoexcited electrons, which are becoming more and more localized near the surface with increasing sheet density of photoexcited charge carriers $N_L$, i.e., with increasing laser fluence $F_L$, due to shortening of the Debye length $l_{\text{Debye}}(N_L) \propto 1/N_L \propto 1/F_L$. We estimated $l_{\text{Debye}}(N_L) \approx 4[N_L/(10^{12}\,\text{cm}^{-2})]^{-1}\,\text{nm} \approx 4[F_L/(1\,\mu\text{J}\,\text{cm}^{-2})]^{-1}\,\text{nm}$. The Debye length importantly exceeds, more than twice, the optical penetration depth of the pump laser if $F_L \leqslant 0.14\,\mu\text{J}\,\text{cm}^{-2}$. For larger fluences the spatial distribution of holes cannot be considered as being much narrower than the spatial distribution of electrons even during the time of their non-ambipolar flow.

The stationary state described by Eq. (B3) is due to the compensation of the electrons' diffusion from the surface by their drift towards the surface from the electric field created by the electrons' and holes' separation. Consequently the characteristic separation time $\tau_{\text{sep}}$ of the charges can be estimated as the drift time of the electrons across the Debye length at a characteristic velocity $\upsilon_{\text{dr},e}$:

$$\tau_{\text{sep}} \approx \frac{l_{\text{Debye}}(N_L)}{\upsilon_{\text{dr},e}} \approx \frac{l_{\text{Debye}}(N_L)}{\mu_e E_{h0}} = \frac{N_L/n_e(\infty)}{\mu_e E_{h0}}$$
$$= \frac{N_L/n_e(\infty)}{\mu_e[|q|N_L/(\epsilon_0\epsilon_r)]} = \frac{\epsilon_0\epsilon_r}{\mu_e |q| n_e(\infty)}$$
$$\equiv \tau^e_{\text{Maxwell}}(N_L). \quad \text{(B4)}$$

The separation time can be identified as the classical Maxwell relaxation time [27,35] for the electrons with the concentration equal to their characteristic concentration $n_e(\infty) \propto N_L^2$ in the stationary distribution of Eq. (B3). The estimates provide $\tau^e_{\text{Maxwell}} = 0.5[N_L/(10^{12}\,\text{cm}^{-2})]^{-2}\,\text{fs} \approx 0.5[F_L/(1\,\mu\text{J}\,\text{cm}^{-2})]^{-2}\,\text{fs}$.

The assumed hole immobility in the derivation of Eq. (B3) during the above evaluated separation process is ensured by the inequality $\tau^e_{\text{Maxwell}} \ll \tau^h_{\text{Maxwell}}$, where the Maxwell relaxation time of the holes is $\tau^h_{\text{Maxwell}} = (\mu_e/\mu_h)\tau^e_{\text{Maxwell}} \approx 15\tau^e_{\text{Maxwell}} \approx 7.5[F_L/(1\,\mu\text{J}\,\text{cm}^{-2})]^{-2}\,\text{fs}$. Qualitatively speaking, there is always more than an order of magnitude difference between the time when the flow of the electrons stops and the motion of the holes becomes important. With the help of this estimate the laser fluence interval can be established $0.01\,\mu\text{J}\,\text{cm}^{-2} \leqslant F_L \leqslant 0.05\,\mu\text{J}\,\text{cm}^{-2}$, where the inequality $\tau^e_{\text{Maxwell}} \leqslant 3.3\,\text{ps} \leqslant \tau^h_{\text{Maxwell}}$ holds, and the distributions described by Eq. (B3) can be considered, from the hypersound generation point of view, as being stationary after their instantaneous creation at $t = 0$. In the considered fluence interval the maximum induced electric fields can be estimated, using $E_{h0} \approx 140[F_L/(1\,\mu\text{J}\,\text{cm}^{-2})]\,\text{kV/cm}$, as $1.4\,\text{kV/cm} \leqslant E_{h0} \leqslant 7\,\text{kV/cm}$. The drift velocities of the electrons can be estimated as $0.8 \times 10^5\,\text{m/s} \leqslant \upsilon_{\text{dr},e} \leqslant 4 \times 10^5\,\text{m/s}$ and the drift velocities of the holes as $0.05 \times 10^5\,\text{m/s} \leqslant \upsilon_{\text{dr},h} \leqslant 0.25 \times 10^5\,\text{m/s}$. The drift velocities of the electrons are supersonic and of the holes subsonic. From the acoustic point of view this is an additional argument to assume instantaneous separation of the electrons from the holes. In other words the electrons cross the charge separation region before the lattice motion starts.

The complete description of the system evolution in this regime, sufficient for the description of hypersound generation at Brillouin angular frequency $\omega$, follows::

$$n_e(z,t) = \frac{N_L/l_{\text{Debye}}}{[1 + z/l_{\text{Debye}}]^2} H(t),$$
$$n_h(z,t) = N_L \delta(z) H(t), \quad \text{(B5)}$$
$$E(t,z) = \frac{E_{h0}}{1 + z/l_{\text{Debye}}} H(t).$$

As has been described earlier in case of an n-doped sample [20], the holes which are $\delta$-localized near the mechanically free surface of the sample have a negligible contribution to the hypersound generation by DP mechanism. The evaluation of the profiles of the longitudinal acoustic pulses generated by the laser-induced stresses $\sigma_{\text{PE}} = -p_E E$ and $\sigma_{\text{DP}} \simeq -d_e n_e$, using the mathematical formalism described in [3,4], leads to:

$$\eta_{\text{PE}}(\tau) = \frac{\left[p_E E_{h0}/\left(2\rho\upsilon_a^2\right)\right]}{1 + (\upsilon_a|\tau|)/l_{\text{Debye}}} \text{sgn}(\tau), \quad \text{(B6)}$$

$$\eta_{\text{DP}}(\tau) = \frac{d_e[N_L/l_{\text{Debye}}]/\left(2\rho\upsilon_a^2\right)}{[1 + (\upsilon_a|\tau|)/l_{\text{Debye}}]^2} \text{sgn}(\tau), \quad \text{(B7)}$$

where $\tau = t - z/\upsilon_a$ and $\upsilon_a$ is the acoustic speed. The evaluation of the spectral component of the laser-generated strain at the Brillouin angular frequency $\omega$ gives

$$\tilde{\eta}^*_{\mathrm{PE}}(\omega) = -i\frac{p_E E_{h0}\tau_{\mathrm{Debye}}}{\rho\upsilon_a^2} f(\omega\tau_{\mathrm{Debye}}), \tag{B8}$$

$$\tilde{\eta}^*_{\mathrm{DP}}(\omega) = -i\frac{d_e N_L}{\rho\upsilon_a^3}(\omega\tau_{\mathrm{Debye}})g(\omega\tau_{\mathrm{Debye}}). \tag{B9}$$

Here $f(x) = \mathrm{Ci}(x)\sin(x) - [\mathrm{Si}(x) - \pi/2]\cos(x)$ and $g(x) = -\mathrm{Ci}(x)\cos(x) - \mathrm{Si}(x)\sin(x)$ are auxiliary functions for sine $[\mathrm{Si}(x)]$ and cosine $[\mathrm{Ci}(x)]$ integrals [36]. The solutions expressed in Eqs. (B8) and (B9) provide opportunity to estimate the relative importance of the PE and DP optoacoustic mechanisms of excitation:

$$\left|\frac{\tilde{\eta}^*_{\mathrm{PE}}(\omega)}{\tilde{\eta}^*_{\mathrm{DP}}(\omega)}\right| = \frac{|p_E|E_{h0}\upsilon_a}{d_e N_L\omega}\left(\frac{f(\omega\tau_{\mathrm{Debye}})}{g(\omega\tau_{\mathrm{Debye}})}\right) = \frac{|p_E||q|\upsilon_a}{\epsilon_0\epsilon_{\mathrm{r}} d_e\omega}\left(\frac{f(\omega\tau_{\mathrm{Debye}})}{g(\omega\tau_{\mathrm{Debye}})}\right). \tag{B10}$$

In accordance with Eq. (B10) the relative efficiency of the two mechanisms depends on the laser fluence through the nondimensional parameter $\omega\tau_{\mathrm{Debye}} \propto 1/N_L$. For the non-ambipolar regime the Debye screening time is long in comparison with the Brillouin period, and the relation (B10) should be analyzed only under the condition $\omega\tau_{\mathrm{Debye}} > 1$. In practice, for $x \geqslant 3$ the auxiliary functions can be approximated by [36] $f(x) \simeq 1/x$ and $g(x) \simeq 1/x^2$. A good estimate for the relative efficiency, valid up to $F_L \approx 0.05\,\mu\mathrm{J\,cm^{-2}}$, is

$$\left|\frac{\tilde{\eta}^*_{\mathrm{PE}}(\omega)}{\tilde{\eta}^*_{\mathrm{DP}}(\omega)}\right| \approx \frac{|p_E||q|}{\epsilon_0\epsilon_{\mathrm{r}} d_e}\tau_{\mathrm{Debye}} \approx 8\,[F_L/(1\,\mu\mathrm{J\,cm^{-2}})]^{-1}. \tag{B11}$$

This estimate predicts that the inverse PE completely dominates the optoacoustic transformation in the investigated asymptotic low-fluence regime.

### 2. Transition from non-ambipolar flow to ambipolar diffusion of the electron-hole plasma

When $F_L \geqslant 0.05\,\mu\mathrm{J\,cm^{-2}}$ the holes cannot be considered as immobile, and when $F_L \geqslant F'_L \approx 0.14\,\mu\mathrm{J\,cm^{-2}}$ it is impossible to neglect the width $1/\alpha$ of the hole distribution, because the inequality $l_{\mathrm{Debye}} \gg 1/\alpha$ does not hold. Moreover the electron distribution is actually not separated spatially from the distribution of holes. When $F_L \geqslant F'_L$ the following condition from the classical theory

$$l_{\mathrm{loc}}(z,t) = |n(z,t)/[\partial n(z,t)/\partial z]| \geqslant l_{\mathrm{Debye}}(z,t)/2 \tag{B12}$$

required for the ambipolar diffusion of the electrons and holes, is satisfied at the vicinity of the semiconductor surface. So, from the physics point of view, for $F_L \geqslant F'_L$ the classical ambipolar diffusion of the electron-hole plasma, characterized by $n_e \simeq n_h \equiv n$ and

$$E(z,t) \equiv -\left(\frac{D_e - D_h}{\mu_e - \mu_h}\right)\frac{\partial \ln[n(t,z)]}{\partial z}, \tag{B13}$$

is expected to take place [27,35]. The description of the ambipolar diffusion of the e-h plasma can be importantly simplified taking into account that the diffusion length $l_D \equiv 2\sqrt{Dt}$, where $D = (\mu_e D_e + \mu_h D_h)/(\mu_e + \mu_h)$ is the ambipolar diffusivity of the electron-hole plasma, significantly exceeds the light penetration depth $\alpha^{-1}$ at the characteristic time scale of the Brillouin period. We estimate $l_D(t = 2\pi/\omega) \equiv 2\sqrt{D(2\pi/\omega)} \approx 160\,\mathrm{nm} \gg \alpha^{-1} \approx 14\,\mathrm{nm}$ even for the lowest reported values of the ambipolar diffusivity $D \approx 3.3\,\mathrm{cm^2/s}$ (the ambipolar diffusivity of GaAs is in the range $D = 3$–$13\,\mathrm{cm^2/s}$ [14,33]). Thus, it can be assumed that the e-h plasma is initially $\delta$-localized at the surface $(1/\alpha \to 0)$. The well-known self-similar solution of the diffusion problem in this asymptotic case is [37]

$$n(z,t) = \frac{N_L}{\sqrt{\pi Dt}}\exp\left(-\frac{z^2}{4Dt}\right)H(t). \tag{B14}$$

Then the Dember electric field takes the form

$$E(z,t) = \frac{D_e - D_h}{\mu_e - \mu_h}\left(\frac{z}{2Dt}\right)H(t). \tag{B15}$$

The formal mathematical divergence of the electric field at large distances $z \to \infty$ indicates that the condition in Eq. (B12) is not satisfied at large distances for the electron-hole plasma distribution of Eq. (B14). However, it is straightforward to verify that due to the Gaussian function in Eq. (B14), the conditions for the ambipolar diffusion are well satisfied at distances shorter than $l_c \approx 2a\sqrt{2Dt}$, where the function $a = a(N_L,t) \approx 1.2$ weakly depends both on time and on laser fluence in the complete domain $1\,\mathrm{ps} \leqslant t \leqslant 200\,\mathrm{ps}$, $0.15\,\mu\mathrm{J\,cm^{-2}} \leqslant F_L \leqslant 2\,\mu\mathrm{J\,cm^{-2}}$ of interest for our experiments.

The correct description of the Dember field should take into account that the electric field, which supports the coherent motion of the electrons and holes, penetrates inside the medium together with the diffusing carriers and, consequently, does not exist importantly deeper than the diffusion depth of the carriers. Thus we obtain

$$E(z,t) = \frac{D_e - D_h}{\mu_e - \mu_h}\left(\frac{z}{2Dt}\right)[H(z) - H(z - l_c(t))]H(t). \tag{B16}$$

The evaluation of the generated acoustic wave at the Brillouin frequency in the regime of the ambipolar diffusion of the electron-hole plasma leads to the following result:

$$\tilde{\eta}^*_{\mathrm{DP}}(\omega) \simeq -N_L\frac{(d_e + d_h)}{\rho\upsilon_a^3}\frac{1}{\sqrt{i\bar{\omega}}}\frac{1}{(1 + i\bar{\omega})}, \tag{B17}$$

$$\tilde{\eta}^*_{\mathrm{PE}}(\omega) = \left(\frac{D_e - D_h}{\mu_e - \mu_h}\right)\frac{p_E a\sqrt{\bar{\omega}}}{\rho\upsilon_a^3}\sqrt{\frac{\pi}{2}} \times\left[1 - \frac{i}{2}\left(\cos(a^2/2\bar{\omega}^2) + \frac{\sqrt{\pi\bar{\omega}}}{a}C(a/\sqrt{\pi\bar{\omega}})\right)\right], \tag{B18}$$

where $\bar{\omega} \equiv \omega_D/\omega$, $\omega_D \equiv \upsilon_a^2/D$, is the characteristic frequency, above which the ambipolar diffusion is supersonic, and $C$ denotes the Fresnel integral [36]. Note that the solution in Eq. (B18) predicts the signal, which only weakly depends on the laser fluence through the parameter $a = a(N_L,t)$, confirming the saturation of the hypersound generation through inverse PE. The velocity of the diffusion wave at

the Brillouin angular frequency $\upsilon_D = \sqrt{D\omega}$ is supersonic, i.e., $\upsilon_D \geqslant 10^4$ m/s $> \upsilon_a = 4.7 \times 10^3$ m/s, even at the lowest reported values of the ambipolar diffusivity [36]. Consequently Eqs. (B17) and (B18) can be evaluated under the condition $\bar{\omega} \ll 1$. The solutions predict that the contribution of the DP mechanism $|\tilde{\eta}_{DP}(\omega)|$ becomes equal to the inverse PE $|\tilde{\eta}_{PE}(\omega)|$ right after the transition to ambipolar diffusion at $F_L'' \approx 0.18\ \mu$J/cm$^2 > F_L' \approx 0.14\,\mu$J/cm$^2$. Qualitatively speaking, the PE generation practically saturates at the transition to ambipolar diffusion, as could have been expected from the functional dependence of the Dember field on the photoexcited carrier concentration in Eq. (B13), i.e., $E_{Dember} \propto \partial \ln(n)/\partial z$, while the contribution to the acoustic field from the DP mechanism keeps growing in amplitude. This finally leads to mutual compensation of two considered contributions on face A(111).

The theory predicts that in the transition from the acoustic strain due to PE described in Eq. (B6) to that due to DP mechanism in Eq. (B17) the optoacoustic excitation efficiency, defined as being proportional to $\partial|\tilde{\eta}(\omega)|/\partial F_L$, diminishes 5–50 times depending on the values of the ambipolar diffusivity. This prediction is in agreement with the experimental observations presented in Figs. 3(b) and 3(c), where the efficiency falls approximately 20 times when the pump laser fluence increases from $F_L \leqslant 0.05\,\mu$J/cm$^2$ up to $F_L \geqslant 0.9\,\mu$J/cm$^2$.


[1] E. Gamaly, *Femtosecond Laser-Matter Interaction: Theory, Experiments, and Applications* (Pan Stanford, Singapore, 2011).

[2] C. Thomsen, H. T. Grahn, H. J. Maris, and J. Tauc, Phys. Rev. B **34**, 4129 (1986).

[3] V. Gusev, Phys. Status Solidi B **158**, 367 (1990).

[4] S. A. Akhmanov and V. E. Gusev, Sov. Phys. Usp. **35**, 153 (1992).

[5] R. Merlin, Solid State Commun. **102**, 207 (1997).

[6] G. W. Chern, C.-K. Sun, G. D. Sanders, and C. J. Stanton, in *Ultrafast Dynamical Processes in Semiconductors*, edited by K.-T. Tsen (Springer-Verlag, Berlin, 2004).

[7] C.-K. Sun, J.-C. Liang, and X.-Y. Yu, Phys. Rev. Lett. **84**, 179 (2000).

[8] Y.-K. Huang, G.-W. Chern, C.-K. Sun, Y. Smorchkova, S. Keller *et al.*, Appl. Phys. Lett. **79**, 3361 (2001).

[9] E. Makarona, B. Daly, J.-S. Im, H. Maris, and A. Nurmikko, Appl. Phys. Lett. **81**, 2791 (2002).

[10] J. S. Yahng, Y. D. Jho, K. J. Yee, E. Oh, J. C. Woo *et al.*, Appl. Phys. Lett. **80**, 4723 (2002).

[11] Y.-C. Wen, L.-C. Chou, H.-H. Lin, V. Gusev, K.-H. Lin *et al.*, Appl. Phys. Lett. **90**, 172102 (2007).

[12] D. M. Moss, A. V. Akimov, A. J. Kent, B. A. Glavin, M. J. Kappers *et al.*, Appl. Phys. Lett. **94**, 011909 (2009).

[13] P. J. S. van Capel, D. Turchinovich, H. P. Porte, S. Lahmann, U. Rossow, A. Hangleiter, and J. I. Dijkhuis, Phys. Rev. B **84**, 085317 (2011).

[14] O. B. Wright, B. Perrin, O. Matsuda, and V. E. Gusev, Phys. Rev. B **64**, 081202 (2001).

[15] O. Matsuda, O. B. Wright, D. H. Hurley, V. E. Gusev, and K. Shimizu, Phys. Rev. Lett. **93**, 095501 (2004).

[16] K.-H. Lin, C.-T. Yu, Y.-C. Wen, and C.-K. Sun, Appl. Phys. Lett. **86**, 093110 (2005).

[17] Y.-C. Wen, T.-S. Ko, T.-C. Lu, H.-C. Kuo, J.-I. Chyi, and C.-K. Sun, Phys. Rev. B **80**, 195201 (2009).

[18] P. Babilotte, P. Ruello, G. Vaudel, T. Pezeril, D. Mounier, J.-M. Breteau, and V. Gusev, Appl. Phys. Lett. **97**, 174103 (2010).

[19] P. Babilotte, P. Ruello, D. Mounier, T. Pezeril, G. Vaudel, M. Edely, J-M. Breteau, V. Gusev, and K. Blary, Phys. Rev. B **81**, 245207 (2010).

[20] P. Babilotte, P. Ruello, T. Pezeril, G. Vaudel, D. Mounier, J.-M. Breteau, and V. Gusev, J. Appl. Phys. **109**, 064909 (2011).

[21] C. S. Kim, J. H. Kim, H. Jeong, Y. D. Jho, H. K. Kwon *et al.*, Appl. Phys. Lett. **100**, 101105 (2012).

[22] C.-C. Chen, H.-M. Huang, T.-C. Lu, H.-C. Kuo, and C.-K. Sun, Appl. Phys. Lett. **100**, 201905 (2012).

[23] D. Daranciang, M. J. Highland, H. Wen, S. M. Young, N. C. Brandt *et al.*, Phys. Rev. Lett. **108**, 087601 (2012).

[24] H. Wen, P. Chen, M. P. Cosgriff, D. A. Walko, J. H. Lee *et al.*, Phys. Rev. Lett. **110**, 037601 (2013).

[25] H. Dember, Phys. Z. **32**, S554 (1931).

[26] T. Dekorsy, H. Auer, C. Waschke, H. J. Bakker, H. G. Roskos, H. Kurz, V. Wagner, and P. Grosse, Phys. Rev. Lett. **74**, 738 (1995).

[27] S. M. Sze and K. K. Ng, *Physics of Semiconductor Devices* (John Wiley & Sons, Hoboken, 2007).

[28] S. Adachi, *GaAs and Related Materials: Bulk Semiconducting and Superlattice Properties* (World Scientific, Singapore, 1994).

[29] P. R. Poulin and Keith A. Nelson, Science **313**, 1756 (2006).

[30] T. Pezeril, C. Klieber, S. Andrieu, and K. A. Nelson, Phys. Rev. Lett. **102**, 107402 (2009).

[31] V. E. Gusev and L. M. Makarova, Akust. Zh. **18**, 683 (1992) [Sov. Phys. Acoust. **38**, 377 (1992)].

[32] S. L. Chuang, *Physics of Optoelectronic Devices* (John Wiley & Sons, Inc., New York, 1995).

[33] *Semiconductors. Physics of Group IV Elements and III-V Compounds*, edited by K.-H. Hellwege and O. Madelung, Landolt-Börnstein, New Series, Group III, Vol. 17, Pt. A (Springer-Verlag, Berlin, 1982).

[34] R. M. Martin, Phys. Rev. B **5**, 1607 (1972).

[35] K. Seeger, *Semiconductor Physics. An Introduction* (Springer-Verlag, Berlin, 1982).

[36] Edited by M. Abramowitz and I. A. Stegun, *Handbook of Mathematical Functions with Formulas, Graphs, and Mathematical Tables* (Dover, New York, 1970).

[37] J. R. Cannon, *The One-Dimensional Heat Equation* (Addison-Wesley, Reading, 1984).